Crystal structure, electronic structure, and vibrational properties of *M*AlSiH (*M*=Ca,Sr,Ba): Hydrogenation-induced semiconductors from the AlB_2-type alloys *M*AlSi

Myeong H. Lee,[1] T. Björling,[2] B. C. Hauback,[3] T. Utsumi,[2] D. Moser,[2] D. Bull,[4] D. Noréus,[2] Otto F. Sankey,[1] and Ulrich Häussermann[5]

[1]*Department of Physics, Arizona State University, Tempe, Arizona 85287-1504, USA*

[2]*Department of Structural Chemistry, Stockholm University, SE-10691 Stockholm, Sweden*

[3]*Institute of Energy Technology, NO-2027 Kjeller, Norway*

[4]*Institute for Materials Research, University of Salford, Salford M5 4WT, United Kingdom*

[5]*Department of Chemistry and Biochemistry, Arizona State University, Tempe, Arizona 85287-1604, USA*

(Received 24 April 2008; revised manuscript received 24 September 2008; published 21 November 2008)

Superconducting AlB_2-type silicides CaAlSi, SrAlSi, and BaAlSi (*M*AlSi) absorb hydrogen and form semiconducting monohydrides where hydrogen is exclusively attached to Al. This induces a metal-nonmetal transition which is accompanied with only a minor rearrangement of the metal atoms. We report the synthesis and structure determination of CaAlSiH and BaAlSiH as well as a first-principles study of the electronic structure and vibrational property changes associated with the metal-nonmetal transition. We find that incorporation of H in *M*AlSi removes the partly occupied antibonding π^* band responsible for metallic behavior and turns it into an energetically low-lying Al-H bonding band. The fully occupied bonding π band in *M*AlSi changes to a weakly dispersed band with Si p_z (lone-pair) character in the hydrides, which becomes located below the Fermi level. The soft phonon mode in *M*AlSi pivotal for the superconducting properties stiffens considerably in the hydride. This mode is associated with the out-of-plane Al-Si vibration and is most affected by the formation of the Al-H bond. The mode of the Al-Si in-plane vibration, however, is unaffected, indicating that the Al-Si bond is equally strong in the metallic precursor and the semiconducting hydride. Al-H modes for *M*AlSiH are weakly dispersed. The frequencies of the stretching mode are around 1200 cm^{-1} and virtually invariant to the *M* environment, indicating a covalent but weak Al-H interaction, which is interpreted as a dative bond from hydridic hydrogen to Al [$Al \leftarrow H^{1-}$].

DOI: 10.1103/PhysRevB.78.195209 PACS number(s): 71.30.+h, 61.66.Fn, 71.15.Mb, 71.20.Lp

I. INTRODUCTION

The discovery of superconductivity at 39 K in MgB_2 (Ref. 1) has drawn attention to isostructural intermetallic compounds with the simple AlB_2 structure.[2] In this respect the ternary silicides *M*AlSi (*M*=Ca,Sr,Ba) have shown interesting behavior.[3–8] Here Al and Si atoms are commonly distributed over the site of the boron atoms forming hexagon layers and *M* atoms occupy the "intercalating" position. For CaAlSi and SrAlSi the superconducting temperatures T_c are 7.8 and 5.1 K, respectively, while, remarkably, stoichiometric BaAlSi is not a superconductor above 2 K, but slightly silicon-rich, $BaAl_{0.95}Si_{1.05}$ (T_c=2.8 K). Obviously the *M* component has a strong influence on T_c, which has been empirically related to changes in the hexagonal c/a ratio of the AlB_2 structure.[8]

The detailed crystal structure of *M*AlSi, however, is still discussed because of the difficult discrimination of Al and Si atoms from diffraction experiments. The disordered AlB_2 structure (space group $P6/mmm$) has been disputed in favor of the SrPtSb structure (space group $P\bar{6}m2$) where Al and Si atoms are ordered alternately in the planar hexagon layers.[9] Indeed recent NMR studies suggested the occurrence of both limiting structures in polycrystalline samples of CaAlSi.[10] Depending on preparation conditions single crystals of CaAlSi can be obtained with a perfectly ordered SrPtSb structure,[11] but may also show five- and sixfold superstructures originating from slightly corrugated hexagon layers.[12] Such structural variations, which have a marked influence on the superconducting properties of CaAlSi single-crystal specimens,[13] have not been reported for SrAlSi and BaAlSi.

While the key ingredients to the superconducting properties of MgB_2 are partially occupied σ bonding states that couple strongly to in-plane vibrations of boron,[14] this situation is radically changed for *M*AlSi due to the increased electron count (nine valence electrons) and the higher mass of constituting atoms. For *M*AlSi partially occupied π^* and *M* *d* states in conjunction with a soft mode associated with the out-of-plane Al-Si vibration have been identified as the origin of the superconducting properties.[9,15,16] Furthermore the nine-electron *M*AlSi systems show the ability to react reversibly with hydrogen. For SrAlSi the resulting monohydride has been structurally characterized.[17] SrAlSiH is stoichiometric and displays slightly puckered hexagon nets in which Si and Al atoms are now unambiguously alternately arranged in an ordered way. Hydrogen is exclusively attached to Al, and Al-H bonding is considered to be largely covalent. The incorporation of H in SrAlSi induces only a minor rearrangement of the metal atoms and resembles a topotactic reaction. However, the electronic structure is most profoundly affected. SrAlSiH was found to be a semiconductor with an indirect band gap of 0.63 eV.[17]

Reversible hydrogen-induced metal-nonmetal transitions occur rarely and systems displaying this phenomenon have attracted attention as switchable mirror systems when the nonmetal is a large band-gap semiconductor.[18–21] This is the case for YH_2-YH_{3-x} or LaH_2-LaH_{3-x}, where the dihydrides are good metals, or Mg_2Ni-Mg_2NiH_4. Although the metallic

component absorbs hydrogen near ambient conditions, the transition is usually accompanied with a major reconstruction of the metal-atom arrangement because the nonmetallic state implies the presence of covalently bonded or hydridic hydrogen. Small metal-atom shifts (<0.7 Å) were recently reported for the metal-nonmetal transition in $LaMg_2Ni$-$LaMg_2NiH_7$. However, the hydrogen uptake still causes a lattice distortion and changes the crystal system from orthorhombic to monoclinic.[22] In this respect the formation of *M*AlSiH from *M*AlSi precursors is truly special because the underlying structural changes across the metal-nonmetal transition can be thought as continuous, second-order-like, with metal-atom shifts below 0.3 Å. Herein we report on the synthesis and structure characterization of CaAlSiH and BaAlSiH and investigate the electronic structure and vibrational property changes associated with the *M*AlSi-*M*AlSiH metal-nonmetal transition by first-principles calculations. Of particular interest will be the mechanism of the band-gap opening in the electronic structure and the alteration of the peculiar soft mode in *M*AlSi upon hydrogen uptake.

II. METHODS

A. Experimental

The hydrides *M*AlSiH can be obtained by reacting *M*AlSi with elemental hydrogen. The procedure for SrAlSiH has been reported earlier.[17] All steps of sample preparation were performed in an Ar-filled glove box (H_2O and O_2 concentration <1 ppm). CaAlSi and BaAlSi were prepared by arc-melting stoichiometric mixtures of the pure elements (>99.99%) under a high-purity Ar atmosphere on a water-cooled copper hearth and remelted three times (weight loss was less than 3%). The composition and homogeneity of *M*AlSi samples was confirmed by energy-dispersive x-ray analysis in a JEOL 820 scanning electron microscope. For hydrogenation, the starting materials were pressed into pellets and loaded into corundum crucibles, which were placed into stainless-steel autoclaves.

Similar to SrAlSi the hydrogenation of BaAlSi was performed with hydrogen pressures between 50 and 90 bar and temperatures above 500 °C. Autoclaves were typically left at these conditions for 1–2 days. The formation of CaAlSiH is more difficult to achieve because the hydrogenation reaction $CaAlSi+\frac{1}{2}H_2 \rightarrow CaAlSiH$ appears to compete with the decomposition reaction $2CaAlSiH+H_2 \rightarrow CaH_2+CaAl_2Si_2$. Best results were obtained when CaAlSi was hydrogenated at 500 °C for 40 min and 50 bar of hydrogen pressure. However, according to powder x-ray-diffraction (PXRD) patterns CaAlSiH samples prepared at these conditions still contained about 10% of $CaAl_2Si_2$ and diffraction lines are considerably broader compared to those for SrAlSiH and BaAlSiH samples. CaH_2 is not detectable by PXRD and is presumably amorphous. For neutron-powder-diffraction (NPD) studies batches of about 3 g of the deuteride BaAlSiD (CaAlSiD) were prepared by reacting BaAlSi (CaAlSi) with deuterium at a pressure of 50 bar (40 bar) and a temperature of 700 °C (500 °C) for 4 days (40 min). SrAlSiH and BaAlSiH may also be obtained by reacting mixtures of MH_2, Al, and Si in a hydrogen atmosphere at temperatures around 700 °C. In this case samples need to be ground to powders and subsequently pressed to pellets several times during the synthesis to achieve a complete reaction. This strategy was applied to prepare a sample (about 3 g) of BaAlSiH for inelastic neutron scattering (INS).

TABLE I. Lattice parameters for *M*AlSi, *M*AlSiH, and *M*AlSiD (in brackets) obtained from x-ray powder-diffraction data.

	CaAlSi	SrAlSi	BaAlSi
a (Å)	4.1902(4)	4.2367(7)	4.3026(6)
c (Å)	4.3994(6)	4.7442(9)	5.1441(9)
c/a	1.051	1.120	1.197
V (Å^3)	66.89	75.15	82.47
	CaAlSiH[D]	SrAlSiH[D]	BaAlSiH[D]
a (Å)	4.1278(7)	4.2139(3)	4.3186(4)
	[4.1316(7)]	[4.2113(3)]	[4.3087(6)]
c (Å)	4.7618(9)	4.9550(6)	5.2080(9)
	[4.766(1)]	[4.9518(5)]	[5.203(1)]
c/a	1.153	1.176	1.206
	[1.153]	[1.176]	[1.208]
V (Å^3)	70.27	76.20	84.12
	[70.45]	[76.05]	[83.66]

The AlB_2-type starting materials and hydrides were characterized by PXRD (Guinier Hägg camera with Cu $K\alpha_1$ radiation; Si was used as internal standard). Lattice parameters were obtained from least-squares refinement of the corresponding diffractograms with the program PIRUM (Ref. 23) and are assembled in Table I. Atomic position parameters of BaAlSiD and CaAlSiD (Table II) were determined from Rietveld profile refinements of NPD data measured at Kjeller, Institute for Energy Technology (IFE), Norway (room temperature, $\lambda=1.5554$ Å) using the program FULLPROF.[24] The Rietveld fits are shown in Fig. 1. For CaAlSiD, diffraction peaks are broader than for BaAlSiD and, moreover, inherently broadened in a peculiar anisotropic way: (00l) reflections are about twice as broad as (hk0) reflections, and (hkl) reflections are in between. This feature indicates stacking disorder and was accounted for by refining the crystal size parameter as implemented in FULLPROF, which improved the peak fitting. The peak of the (101) reflection (around $2\theta=30°$), however, remained somewhat poorly fitted ($R_{\mathrm{Bragg}}=4.99\%$ and $R_f=2.51\%$). The BaAlSiD sample contained some small unidentified impurity peaks, mainly in the region $35° < 2\Theta < 45°$ ($R_{\mathrm{Bragg}}=5.43\%$ and $R_f=4.70\%$).

The INS spectrum of BaAlSiH was measured at 20 K on the high-resolution time-of-flight spectrometer TOSCA at the pulsed neutron spallation source ISIS (Rutherford Appleton Laboratory, U.K.), accessing an energy transfer from 0 to 4000 cm^{-1}. The spectrum revealed a small amount of BaH_2 from the initial synthesis as an impurity.

B. Calculational

Theoretical calculations were performed using the local-density approximation within the density-functional theory

TABLE II. Atomic position parameters of BaAlSiD and CaAlSiD (space group $P3m1$, No. 156) determined from Rietveld profile refinements of neutron-powder-diffraction data. $B=8\pi^2U_{iso}$ (Å^2). For SrAlSiD z(Al)=0.547(1), z(Si)=0.431(2), and z(H)=0.904(1) (Ref. 17).

Atom	Site	x	y	z	B	Occ.
Ba	1a	0	0	0	0.6(1)	1
Al	1c	2/3	1/3	0.535(2)	1.1(2)	1
Si	1b	1/3	2/3	0.449(2)	0.7(2)	1
D	1c	2/3	1/3	0.868(2)	1.4(1)	1

Atom	Site	x	y	z	B	Occ.
Ca	1a	0	0	0	1.1(2)	1
Al	1c	2/3	1/3	0.548(5)	0.4(1)	1
Si	1b	1/3	2/3	0.462(2)	0.4(1)	1
D	1c	2/3	1/3	0.915(5)	3.6(2)	1

(DFT) and a plane-wave basis set as implemented in the program VASP.[25] The exchange-correlation energy was approximated with the generalized gradient approximation (GGA) of Perdew and Wang.[26] Ultrasoft pseudopotentials (PPs) and the frozen-core all-electron projector augmented wave (PAW) method were used.[27,28] The cell parameters and the atoms' positions were optimized for a fixed volume of the unit cell. For MAlSi the Al/Si ordered arrangement (space group $P\bar{6}m2$) corresponding to the 1H polymorph was considered. By repeating this process for different volumes, we obtain the equation of state, and the optimum cell parameters are determined from the global minimum energy. Using the optimized cell parameters and volume, the internal coordinates of the atoms in the unit cell were relaxed again to a higher tolerance to have zero force. The obtained structural parameters are listed in Table III. Charge densities including the core charges were calculated with the PAW method.

The phonon-dispersion curves were obtained using a direct method[29,30] with supercells. A $3a\times3a\times3c$ supercell was generated, and the internal coordinates of all the atoms in the supercell were relaxed using a $3\times3\times3$ k-point sampling until the forces converged to less than 0.1 meV/Å (PP calculations). The atoms in the supercell are displaced by 0.01 Å from the equilibrium position along each of the Cartesian directions. We reduced the number of the displaced atoms using symmetry. The Hellmann-Feynman force acting on each atom was computed for each displacement and divided by the displacement to give the force constants. A displacement of a single atom gives the one column of the dynamical matrix. We displaced each atom in both the positive and the negative directions, and averaged the force constants to remove the anharmonicity. A finite range of interaction (less than half the supercell dimensions) is considered to construct the wave-vector-dependent dynamical matrix. The wave-vector-dependent dynamical matrix is diagonalized to give the normal-mode frequency and eigenvectors. We repeated the vibrational frequency calculation for the displacement of 0.02 Å, and the phonon-dispersion curve remained almost the same. More computational details can be found in Ref. 30.

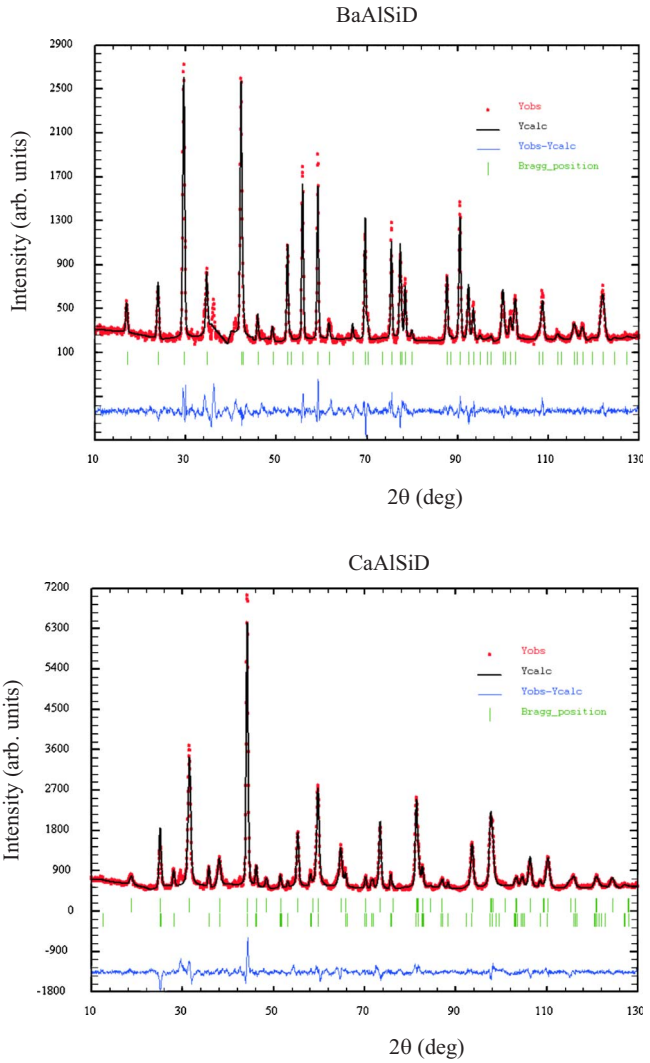

FIG. 1. (Color online) Rietveld fits to the neutron-powder-diffraction-patterns of BaAlSiD (top; Bragg R factor of 5.43% and R_f factor of 4.70%) and CaAlSiD (bottom; Bragg R factor of 4.99% and R_f factor of 2.51%). The wavelength is 1.5554 Å. Dots represent the observed pattern and the solid line is the calculated pattern.

TABLE III. Computationally relaxed structural parameters of *M*AlSi and *M*AlSiH. PAW values are in brackets.

	CaAlSi	SrAlSi	BaAlSi
a (Å)	4.1931	4.2581	4.3151
	[4.2051]	[4.2627]	[4.3238]
c (Å)	4.3545	4.7540	5.2301
	[4.3789]	[4.7527]	[5.1967]
c/a	1.038	1.116	1.212
	[1.041]	[1.115]	[1.202]
V (Å^3)	66.30	74.65	84.34
	[67.06]	[74.79]	[84.14]
	CaAlSiH	SrAlSiH	BaAlSiH
a (Å)	4.1257	4.2202	4.3416
	[4.1373]	[4.2263]	[4.3271]
c (Å)	4.6945	4.9662	5.2929
	[4.7103]	[4.9613]	[5.2617]
c/a	1.138	1.177	1.219
	[1.139]	[1.174]	[1.216]
V (Å^3)	69.20	76.60	86.40
	[69.82]	[76.74]	[85.32]
z(Al)	0.5428	0.5403	0.5346
	[0.5435]	[0.5407]	[0.5368]
z(H)	0.9164	0.8916	0.8643
	[0.9150]	[0.8939]	[0.8671]
z(Si)	0.4341	0.4451	0.4582
	[0.4336]	[0.4461]	[0.4572]

Using the direct method based on forces obtained with the VASP code led to an imaginary frequency (soft mode) for CaAlSi in the upper part of the Brillouin zone (A-L), which indicates the dynamical instability for this mode. This phenomenon was also observed by Huang *et al.*[16] when employing full-potential linear muffin tin orbitals (FP-LMTO) and linear response to calculate the dynamical matrix. These authors obtained an imaginary frequency at some k points along the A-L direction. The presence of an imaginary frequency for a soft mode in CaAlSi was disputed by Giantomassi *et al.*,[9] who calculated a dispersionless low-frequency mode in the upper part of the Brillouin zone while using a linear-response function approach with the ABINIT code. A similar result was found by Heid *et al.*,[31] who obtained a rather flat dispersion curve along the upper part of the Brillouin zone. At this stage it is not clear why some calculations produce a dynamical instability while others do not. We noticed, however, that the frequency of the soft mode is highly susceptible to c/a ratio variations. Further, Huang *et al.*[32] and Boeri *et al.*[33] showed that the low-frequency mode for CaAlSi becomes softer and an imaginary frequency occurs at a large volume of the Brillouin zone when pressure is increased. We also performed ABINIT computations[34,35] of the phonon dispersion for CaAlSi using the Perdew-Wang-Ceperley-Alder functional to approximate the exchange-correlation and Troullier-Martins pseudopotentials. The Brillouin-zone integration was performed over a $14\times14\times14$ Monkhorst-Pack grid.[36] The result was that the mode remains stable even along the A-L direction, which agrees with the result obtained by Giantomassi *et al.*[9] and also Heid *et al.*[31] and Boeri *et al.*[33] We consider the stable low-frequency mode physically more reasonable, but for the sake of methodological consistency we will present the VASP-direct method result in Sec. III C.

III. RESULTS AND DISCUSSION

A. Hydrogenation-induced structural changes

The AlB_2-type alloys *M*AlSi are part of extended solid solutions $MAl_{2-x}Si_x$ ($\approx0.6<x<\approx1.2$ for M=Ca and Sr and $\approx0.6<x<\approx1.5$ for M=Ba) and have been investigated extensively over the recent years. Our lattice parameters (Table I) are in good agreement with previous reports.[3–8] As mentioned earlier, the actual distribution of Al and Si on the hexagon layer is most difficult to establish experimentally. Although Al and Si may have a tendency to order, it is reasonable to assume that our specimens obtained from high-temperature arc-melting are to a large extent Al/Si disordered. The hydrogenation of *M*AlSi affords SrAlSiH and BaAlSiH as stoichiometric, crystallographically well-ordered materials (SrAlSiH structure; Table II), while CaAlSiH displays considerable stacking disorder along the c direction of the trigonal SrAlSiH basis structure. This disorder is expressed in broader diffraction lines, especially affecting (00l) reflections, and is largely caused by the intrinsic formation and incorporation of blocks of $CaAl_2Si_2$ at the unit-cell level in CaAlSiH crystals. $CaAl_2Si_2$ and CaAlSiH have the same trigonal space group and very similar a lattice parameters. A detailed study of this phenomenon will be published elsewhere.[37] All hydrides are thermally rather stable with atmospheric decomposition temperatures slightly above 600 °C for SrAlSiH and BaAlSiH, and around 500 °C for CaAlSiH.

The structural consequences of the hydrogenation of *M*AlSi to *M*AlSiH are depicted in Fig. 2. Considering the precursors either in the disordered AlB_2 structure ($P6/mmm$) or in the ordered, noncentrosymmetric SrPtSb structure ($P\bar{6}m2$) hydrogenation causes the loss of hexagonal symmetry due to the puckering of Al-Si layers and in *M*AlSiH space-group symmetry is reduced to $P3m1$ [Figs. 2(a) and 2(b)]. The symmetry reduction from the AlB_2 to the SrAlSiH structure can be simply expressed as two consecutive translationengleiche steps of index 2 ($t2$) where ordering implies the loss of the inversion center and puckering implies the loss of the horizontal mirror plane.[38] The introduction of hydrogen changes the coordination number of Al from 3 in *M*AlSi to 4 in *M*AlSiH. Most pronounced, however, is the change in the coordination of M atoms, which are sandwiched in between two Al/Si hexagon rings in *M*AlSi but attain a more rigid environment by three H, three Si, and three Al atoms at shorter distances in the hydride [Figs. 2(c) and 2(d)]. The H atom is coordinated quasitetrahedrally by one Al and three M atoms [Fig. 2(e)].

The calculated structural parameters are generally in good agreement with experiment; PP and PAW results are very

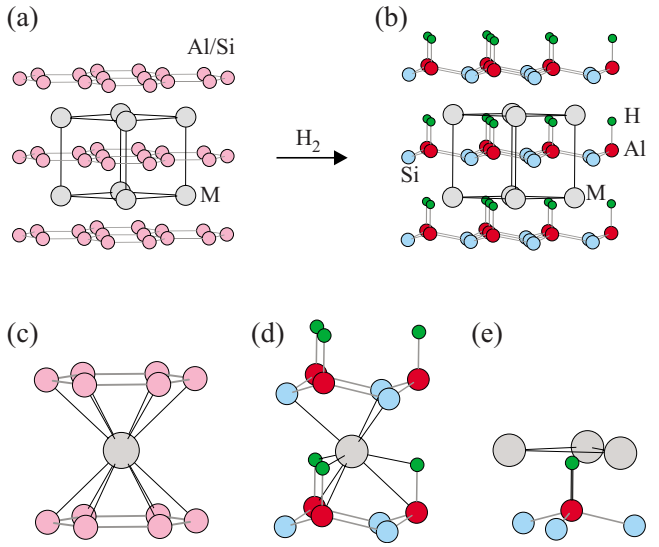

FIG. 2. (Color online) Crystal structures of (a) AlB_2-type MAlSi and (b) SrAlSiH-type MAlSiH. Large gray circles denote alkaline-earth (M) atoms. Red (dark gray)—Al; blue (light gray)—Si; green (small circles)—H. Pink (medium gray) circles indicate an Al/Si disordered site. Local coordinations of M atoms in (c) MAlSi and (d) MAlSiH, and of the H atom in (e) MAlSiH.

TABLE IV. Comparison of experimental and calculated interatomic distances (Å). PAW values are in brackets.

	CaAlSi	SrAlSi	BaAlSi
Al-Si (×3)	2.42 [2.43]	2.47 [2.42]	2.48 [2.50]
Expt.	2.4192(2)	2.4461(4)	2.4841(3)
M-Al/Si (×12)	3.26 [3.27]	3.42 [3.42]	3.61 [3.60]
Expt.	3.2698(3)	3.4074(4)	3.5758(4)
	CaAlSiH	**SrAlSiH**	**BaAlSiH**
Al-Si (×3)	2.44 [2.44]	2.48 [2.49]	2.54 [2.53]
Expt.	2.420(4)	2.498(2)	2.528(3)
M-H (×3)	2.41 [2.42]	2.50 [2.50]	2.61 [2.59]
Expt.	2.420(4)	2.478(1)	2.581(3)
M-Si (×3)	3.13 [3.14]	3.29 [3.29]	3.49 [3.47]
Expt.	3.246(6)	3.237(6)	3.413(7)
M-Al (×3)	3.21 [3.21]	3.34 [3.34]	3.51 [3.49]
Expt.	3.21(2)	3.308(4)	3.470(7)
Al-H (×1)	1.75 [1.75]	1.75 [1.75]	1.75 [1.74]
Expt.	1.75(3)	1.768(9)	1.73(2)

similar (Table III). The largest deviations occur for the c lattice parameter of CaAlSiH, which is underestimated by 1.4%, and the c lattice parameters of BaAlSi and BaAlSiH, which are both overestimated by 1.7% in the PP calculations. In this respect PAW calculations yield slightly improved results. Also, we note a larger discrepancy between experiment and calculations (for both PP and PAW calculations) for the Si-atom position parameter of CaAlSiH. This, however, could be a consequence of the disorder in CaAlSiH and associated shortcomings in the Rietveld refinement of the structure. We also need to point out that for CaAlSiD the experimental lattice parameters (and volume) are larger than for CaAlSiH, which is reverse of the trend typically observed and most likely reflects different degrees of disorder in the hydride and deuteride.

The effect of hydrogenation to the lattice parameters and interatomic distances can be extracted from Tables I and IV. The Al-H distance in MAlSiH is very similar, around 1.75 Å, and thus does not depend on the alkaline-earth metal environment. The M-H distances in MAlSiH correspond well to the shortest M-H distances in the MH_2 salts with the cotunnite structure when M=Sr and Ba.[39,40] The Ca-H distance in CaAlSiH (2.42 Å) is however considerably longer than the shortest distances in CaH_2 (2.17–2.33 Å).[39] Intuitively, when comparing the AlB_2 and SrAlSiH structures [Figs. 2(a) and 2(b)], hydrogenation is expected to affect (increase) the c/a ratio. This is indeed the case for M=Ca, but the increase diminishes for M=Sr and is virtually absent for M=Ba. Remarkable is the very small unit-cell volume increase for M=Sr and Ba connected with hydrogen uptake (around 2%, or below 1.5 $Å^3$/hydrogen), which is attributed to the effective coordination of H by the M component (i.e., M-H distances as in MH_2). Interestingly, the typically observed phenomenon that metal hydrides are obtained as fine powders when hydrogenating intermetallic precursors is not the case for MAlSiH. Crystals, ingots, or pellets of MAlSi preserve their shape upon hydrogenation. For transition-metal-based intermetallic hydrides an average volume expansion of around 3 $Å^3$/H atom is often observed.[41] For main-group metal-based systems large fluctuations occur. Typically, for alkali metals and heavier alkaline-earth metals (Ca-Ba) hydride formation is accompanied with a substantial volume reduction. For Mg-MgH_2, however, there is a volume increase of 7.5 $Å^3$/H atom. For H in mixed s- and p-element environments, there are much less data. In the case of CaSi-CaSiH a volume expansion of about 15 $Å^3$/H atom has been reported,[42] whereas small negative volume effects were observed for systems such as Ca_5Sb_3-Ca_5Sb_3H.[43] For MAlSi→MAlSiH the Al-Si interatomic distance increases only slightly upon puckering of the hexagon layers (by 0.02, 0.03, and 0.04 Å for M=Ca, Sr, and Ba, respectively).

B. Electronic structure changes

The calculated band structures and density of states (DOS) are shown in Figs. 3 and 4, respectively. The electronic structures of MAlSi are in good agreement with previous calculations where they have been compared to MgB_2.[9,15,16,44] Here we analyze them with respect to MAlSiH.

In MAlSi the Al and Si s, p_x, and p_y orbitals form three bonding σ bands which are occupied (Fig. 3, left panel). The lowest-lying σ band is essentially composed of Si s orbitals and energetically detached from the other two σ bands. The Al and Si p_z orbitals give rise to two π bands, one bonding and one antibonding. Due to the different energies of Al and Si p_z orbitals, the bonding π band has a larger Si p_z contri-

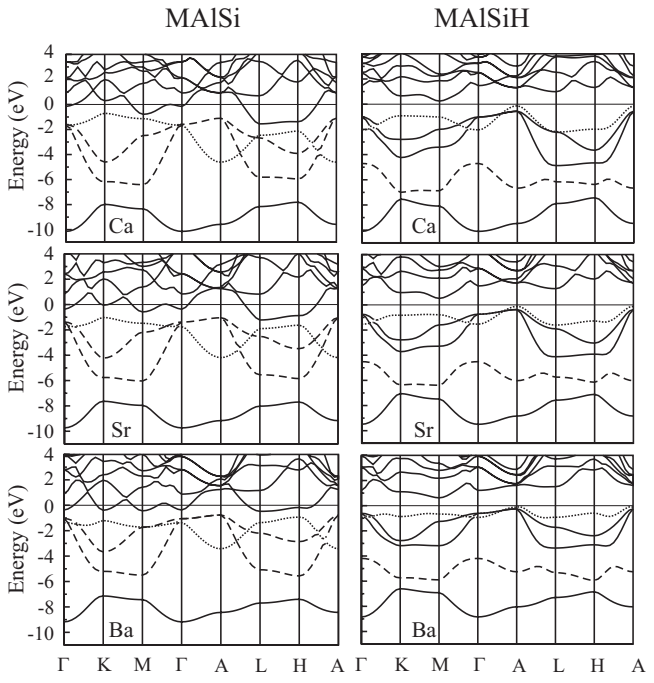

FIG. 3. Electronic band structures of *M*AlSi (left panel) and *M*AlSiH (right panel). For *M*AlSi the occupied π band is indicated as dotted line, and the two p orbital–based σ bands are indicated as dashed lines. For *M*AlSiH the Si p_z band is indicated as dotted line and the H s-dominated band as dashed line.

bution and, vice versa, the antibonding π^* band has a larger Al p_z contribution. As a consequence the bonding π band is very weakly dispersed in the reciprocal plane Γ-*K*-*M* but sizably dispersed along Γ-*A*. This is different from MgB_2, which has homonuclear boron layers. For the nine-electron *M*AlSi systems, the Al p_z-based π^* band becomes partially occupied. This is especially the case along *L*-*H*. Additionally a *M* d band with mainly d_{z2} character crosses the Fermi level (along Γ-*M* and Γ-*K*).[9,16] When going from CaAlSi to BaAlSi, bands become less dispersed because of the increase in unit-cell volume. At the same time the DOS at the Fermi level, $N(E_F)$, increases from 1.054 to 1.339 to 1.578 (Fig. 4, left panel). The DOS shows further that the π-π^* splitting becomes more pronounced with increasing mass of *M*, and in BaAlSi even a gap occurs between these two bands which is located at about −0.8 eV below the Fermi level. The partial DOS for Si p_z and Al p_z orbitals shows their asymmetric distribution in the bonding and antibonding π bands. The contribution of *M* states to the occupied bands is comparable in the three *M*AlSi systems. We find that the integrated values within spheres based on the respective ionic radii of *M* are very similar.[45]

In the hydrides *M*AlSiH an indirect band gap is opened whose size increases from about 0.3 to 0.8 eV when going from *M*=Ca to Ba (Figs. 3 and 4, right panels). For SrAlSiH our DOS and band structure are similar to those in previous reports.[17,46] We emphasize the Al p_z, Si p_z, and H s orbital characters of the five valence bands. The Si p_z orbitals form a flatband below the Fermi level; its small dispersion becomes especially pronounced in BaAlSiH. The lowest-lying band in *M*AlSiH stems from Si s orbitals and displays the

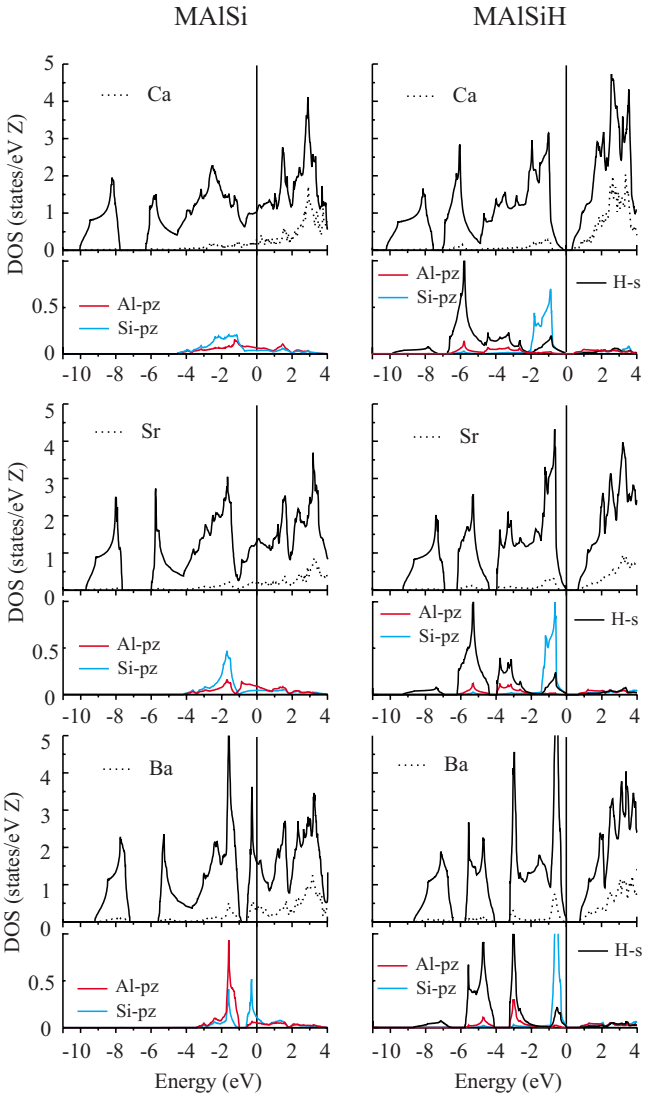

FIG. 4. (Color online) DOSs for *M*AlSi (left panel) and *M*AlSiH (right panel). The *M* (s,p,d)-projected DOS is shown as dotted line. Al p_z-, Si p_z-, and H s-projected DOSs are shown as solid red (dark gray), blue (light gray), and black lines, respectively.

same topology and range of energy as in *M*AlSi. The band next in energy has a large H s contribution and a sizable Al s and a minor Al p_z contribution. It is identified as Al-H bonding band. The remaining bands (below the Si p_z band) correspond to the two upper bonding σ bands in *M*AlSi, based on the p_x and p_y orbitals of Al and Si. In *M*AlSiH these bands also contain a sizable H s contribution and, because of the lower symmetry of the puckered layer structure, a sizable Al p_z contribution. We conclude that hydrogen incorporation in *M*AlSi removes the partly occupied antibonding π^* band, which has dominant Al p_z character, through Al-H bond formation. In turn, the fully occupied bonding π band changes to a weakly dispersed band with Si p_z (lone pair) character in the hydride. Compared to the π band in *M*AlSi, the Si p_z lone-pair band in *M*AlSiH is raised in energy on the reciprocal plane Γ-*A*-*L*-*H* (the upper half of the Brillouin zone) and becomes located below the Fermi level. These changes are schematically sketched in Fig. 5. The contribution of *M*

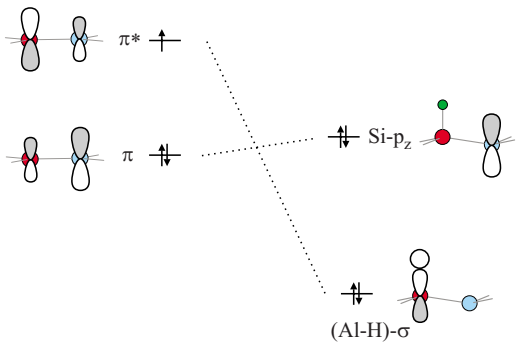

FIG. 5. (Color online) Sketch of the electronic structure change induced by the hydrogenation of *M*AlSi.

states to the occupied bands in *M*AlSiH is similar to that in *M*AlSi. Integrated values within spheres for *M* having the same size are almost identical for pairs of *M*AlSi/*M*AlSiH.[45]

When applying a localized bonding picture, *M*AlSiH corresponds to an electron-precise Zintl phase consisting of a layered polyanion $[AlSiH]^{2-}$ with three-bonded $[Al\text{-}H]^{-}$ and three-bonded, lone-pair-carrying Si^{-} entities. The charge of the polyanion is counterbalanced by M^{2+} cations. The bonding between Al and Si atoms is then considered being of two-center two-electron σ type. In contrast, Al-Si bonding in the graphitic layers of the AlB_2 precursors has a π contribution from the fully occupied bonding and partially occupied antibonding bands. However, the bonding and antibonding characters of the π and π^* bands is weakened by the polarity of the Al-Si bond. Formally the nine-electron *M*AlSi phases represent electron-excess systems with respect to eight-electron main-group AlB_2 compounds (MgB_2, $SrGa_2$, and $BaGa_2$) where only the π bonding band is occupied. With the incorporation of hydrogen, this situation is resolved; the hydrides represent electron-precise semiconductors.

In the following we elaborate on this simple picture of the *M*AlSi→*M*AlSiH transition by analyzing the associated changes in the charge density. Figure 6 compiles the charge-density maps for the $(1\bar{1}0)$ planes containing all atoms in both *M*AlSi and *M*AlSiH structures. For *M*AlSi the expected polar covalent bonding between Al and Si atoms within a hexagon layer is clearly apparent. There is a substantial charge accumulation around Si and the critical points in the charge density between the nuclei are shifted to Al. Density values at the critical point decreases from 0.37 to 0.35 to 0.29 $e/Å^3$ when going from *M*=Ca to Ba, in accord with the increasing Al-Si distances. Interestingly, the incorporation of H does not redistribute charge density associated with Al-Si bonding. The location of the critical point along the Al-Si bond paths and its density value are virtually unchanged in *M*AlSiH. The charge-density maps for *M*AlSiH reveal also clearly covalent Al-H bonding. At the critical point along the Al-H bond paths, density values are around 0.38 $e/Å^3$ and virtually the same for the three compounds. Further noticeable is a considerable charge density in the region between *M* and H and, compared to *M*AlSi, also between *M* and Si. The latter redistribution is induced by the substantial shortening of *M*-Si distances upon puckering of the hexagon layers when going from *M*AlSi to *M*AlSiH [cf. Figs. 2(c) and 2(d)].

While the analysis of the charge density suggests that the *M*AlSiH systems represent Zintl phases where H is part of a polyanion $[AlSiH]^{2-}$, we are still left with the question of the actual nature of the Al-H bond. H represents the most electronegative component in *M*AlSiH and it is reasonable to assume that it occurs hydridic (that is, as H^{-}). This has been pointed out in a recent bonding analysis of SrAlSiH where it was concluded that H and Sr occur as ions that provide charge balance to the layered polyanion $[AlSi]^{-}$.[46] We do not question the occurrence of hydridic H, but instead of considering H^{-} as an isolated ion, we prefer that the H^{-} electron pair is used to form a dative bond to nominally zero-charged Al, i.e., $[Al\leftarrow H^{1-}]$. This is compatible with the charge-density analysis and the band structure where H *s* states are strongly hybridized with Al *s* and Al p_z states in a range between −6.5 and −2 eV. As a consequence Al is involved in four covalent polar bonds, three to Si and one to H. The following analysis of the vibrational properties of *M*AlSiH will further corroborate this view.

C. Vibrational property changes

As analyzed in Sec. III B, hydrogenation leads to band-gap opening in the electronic structure of metallic *M*AlSi.

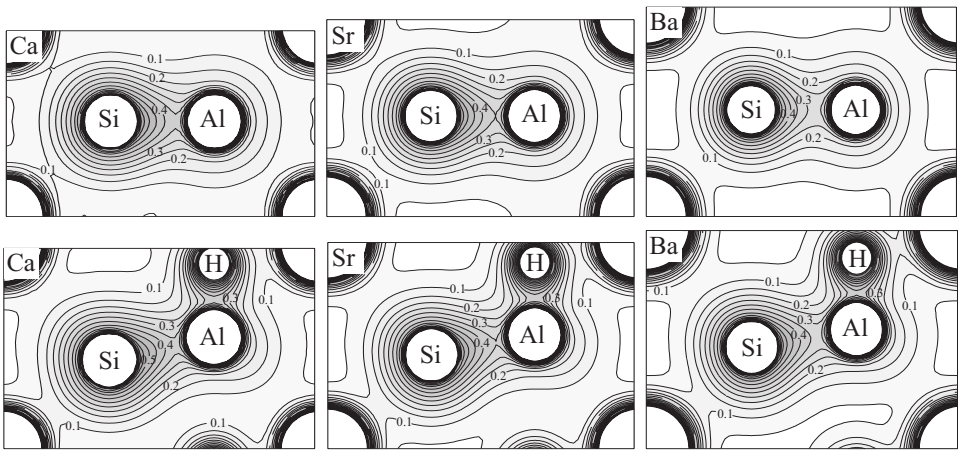

FIG. 6. Charge-density distribution (including core charges) for *M*AlSi and *M*AlSiH on the $(1\bar{1}0)$ plane. The contours are equally spaced in increments of 0.05 $e/Å^3$ and cover a range from 0 to 0.8 $e/Å^3$.

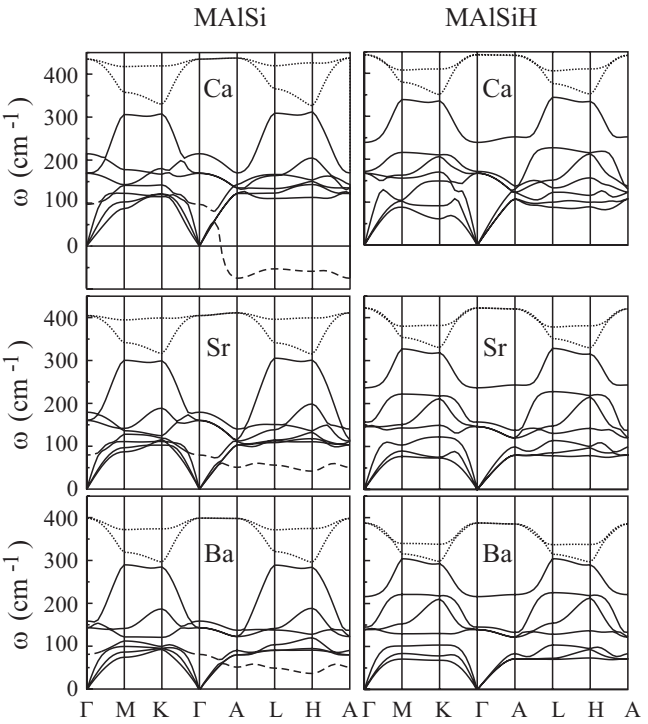

FIG. 7. Calculated phonon-dispersion curves for *M*AlSi (left) and *M*AlSiH (right). The Al-Si in-plane stretching mode is displayed as dotted line and the soft mode in *M*AlSi as dashed line.

Next we turn to the vibrational property changes accompanied with the hydrogenation-induced metal-semiconductor transition. The calculated phonon dispersions for *M*AlSi and *M*AlSiH are shown in Fig. 7 (left- and right-hand panels, respectively). For the hydrides the high-frequency modes involving hydrogen, which have wave numbers above 700 cm^{-1}, are omitted in Fig. 7. Our focus is first on the changes in modes predominantly arising from the metal atoms. We return to the hydrogen-based modes at the end of this section.

The characteristic feature of the *M*AlSi phonon dispersions is the occurrence of a peculiar low-frequency mode (highlighted as dashed line in Fig. 7) which is soft in the upper half of the Brillouin zone (i.e., the boundary $k_z=\pi/c$). This mode plays a major role in the superconducting properties of *M*AlSi by coupling to the Fermi-level electrons in the partially occupied π^* band situated at the same location of the Brillouin zone. Recent spectroscopic and calculational investigations showed that the soft mode for CaAlSi originates from out-of-plane Al-Si vibrations.[31,47] Note that π^* is dominated by Al p_z orbital character. For *M*=Sr and Ba the mode is shifted to higher frequencies and hybridizes with other modes. By this, coupling strength is lost and T_c reduces accordingly.[31] Our phonon dispersions for *M*AlSi are in good agreement with previous calculations,[9,32,33] apart from the fact that soft-mode frequencies obtained were imaginary for CaAlSi and too low for SrAlSi and BaAlSi. A recent study of 1*H*-CaAlSi (the polymorph with the simplest structure) achieved excellent agreement between experimental phonon dispersion obtained by inelastic x-ray scattering and DFT calculations using linear response in combination with the mixed pseudopotential method.[47] It appears that linear response is more appropriate for the investigation of the lattice dynamics of *M*AlSi, although—as already discussed in Sec. II B—the problem may be more complex. However, for our comparative study of the vibrational properties of *M*AlSi and *M*AlSiH, the accurate reproduction of the soft mode in *M*AlSi is less important.

TABLE V. Calculated phonon frequencies (in cm^{-1}) for optical modes at the Γ point (equilibrium lattice parameters).

Mode type	CaAlSi	SrAlSi	BaAlSi
E (*M*;*xy*)	168	160	143
A (*M*;*z*)	230	179	159
A (Al-Si; *z*)	98	79	81
E (Al-Si; *xy*)	435	405	399
Mode type	**CaAlSiH**	**SrAlSiH**	**BaAlSiH**
E (*M*;*xy*)	167	146	139
A (*M*;*z*)	171	157	145
A (Al-Si; *z*)	239	237	216
E (Al-Si; *xy*)	443	422	387
E (Al-H bend)	756	829	865
A (Al-H stretch)	1225	1215	1224

At first sight the phonon dispersions of the hydrides *M*AlSiH look similar to the those of precursors although the soft-mode feature is clearly absent. Considering only the metal atoms (three in the unit cell) will give rise to nine normal modes of vibrations: in addition to the acoustic modes (three) there are six optic modes, which occur as two pairs (*A*+*E*). The symbols *A* and *E* denote generically the main displacements along *z* ("out of plane") and (*x*,*y*) ("in plane"), respectively. They may be characterized as Al and Si atoms displaced along *z* in opposite directions (*A*) and in-plane Al-Si stretching (*E*), and *M* vibrations against (*A*) and along Al-Si layers (*E*). The frequencies of zone-center optical phonons of *M*AlSi and the corresponding hydrides are compiled in Table V. The mode highest in frequency corresponds to the degenerate Al-Si stretching mode and represents a direct measure of the Al-Si in-plane bond strength. Although this mode is dispersed by about 100 cm^{-1} in both the metal and the hydride, it appears separated from the other modes. The zone-center frequency decreases slightly from *M*=Ca to Ba in both series, reflecting the increase in the Al-Si interatomic distance with increasing unit-cell volume (cf. Table V). Most importantly, the mode of the Al-Si in-plane vibration appears virtually unaffected by hydrogen incorporation, indicating that the in-plane Al-Si bond is actually equally strong in the metallic precursor and the semiconducting hydride.

Radically different is the situation for the out-of-plane Al-Si vibration, which is most affected by the formation of the Al-H bond. In *M*AlSi this mode represents the lowest-frequency optical mode. The Γ-point frequencies of this mode are 98 cm^{-1} for *M*=Ca (around 100 cm^{-1} in previous calculations[9,16,31–33]) and around 80 cm^{-1} for *M*=Sr and Ba

(around 115 cm^{-1} in previous calculations[16,32]). As mentioned above, it continues as a dispersionless soft mode in the upper half of the Brillouin zone with frequencies below that of the acoustic modes. In the hydrides this mode is considerably stiffened and Γ-point frequencies attain values above 200 cm^{-1} (cf. Table V). It should be noted that unlike in *M*AlSi the Γ-point displacements of the out-of-plane Al-Si vibration in the hydrides attain a substantial contribution from the *M* atoms; i.e., this mode hybridizes with the *M*-based optic modes. Further, due to the absence of the soft modes in the hydrides, optic modes are separated from the acoustic ones. This feature in the phonon dispersions becomes more pronounced with increasing mass of *M*.

The origin of the soft mode in *M*AlSi is still not clear. It has been argued that the partial filling of π^* bands is responsible for a weakening of the Al-Si bond in the vertical direction.[9] In this respect and in line with the charge-density analysis (cf. Fig. 6), Al-Si bonding is not stronger in the hydrides with exclusively σ-bonded atoms. However, the additional coordination of Al by H rigidizes the vertical out-of-plane vibration of the hexagon layers.

Finally we return to the H-based modes. The experimental INS spectrum of BaAlSiH is shown in Fig. 8(a) for the range between 500 and 2500 cm^{-1}. The corresponding spectrum of SrAlSiH has been reported previously in a comparative study with $SrAl_2H_2$.[48] The experimental INS spectrum of disordered CaAlSiH deviates somewhat from that of the ordered homologs and will be discussed in a forthcoming study.[37]

In the INS spectrum of BaAlSiH the H-based modes give rise to two narrow bands at around 900 and 1200 cm^{-1}, corresponding to Al-H bending and stretching modes, respectively. Additionally well-resolved overtones appear above 1500 cm^{-1}. Thus, the internal Al-H modes (bending *E* and stretching *A*) are clearly separated from the external lattice modes discussed above. In Fig. 8(a) the experimental INS spectrum is compared to a calculated spectrum obtained by the program ACLIMAX by using computed frequencies and displacements across the Brillouin zone and taking into account 0–1 to 0–3 transitions.[49] Originally, the calculated frequencies for the bending mode are underestimated by about 40 cm^{-1} (about 5%), while the frequencies for the stretching mode agree within 10 cm^{-1}. When shifting the calculated frequencies of the bending mode to match the ones in the experimental spectrum and subsequently recalculating the INS spectrum, excellent agreement between calculated and experimental spectra is achieved. This scaling procedure is often performed to make frequencies from first-principles calculations to coincide with experimental ones.[49,50] With agreement between experimental and calculated frequencies, experimental spectra can be unambiguously evaluated. Clearly resolved are the two quanta events around 1800 cm^{-1} (bending-mode overtone), 2100 cm^{-1} (combination mode), and 2300 cm^{-1} (stretching-mode overtone). The latter mode is downshifted by about 100 cm^{-1} compared to the wave number expected from a harmonic behavior ($2 \times 1200\ cm^{-1} = 2400\ cm^{-1}$). A similar anharmonicity for the Al-H stretch has also been detected for SrAlSiH.[48]

Figure 8(b) compiles calculated INS spectra based on the originally computed frequencies (i.e., unshifted) and displacements for all three *M*AlSiH and focusing on the locations of the bending- and stretching-mode bands. See Table V for the calculated Γ-point frequencies. As a major result, the Al-H stretching-mode frequency is virtually invariant to the *M*-atom environment, whereas bending-mode frequencies shift to lower wave numbers when going from BaAlSiH to CaAlSiH. Stretching- and bending-mode frequencies are well separated from each other (by several hundreds of wave numbers), which implies directional (covalent) bonding of H in its tetrahedral environment M_3Al [cf. Fig. 2(e)]. The

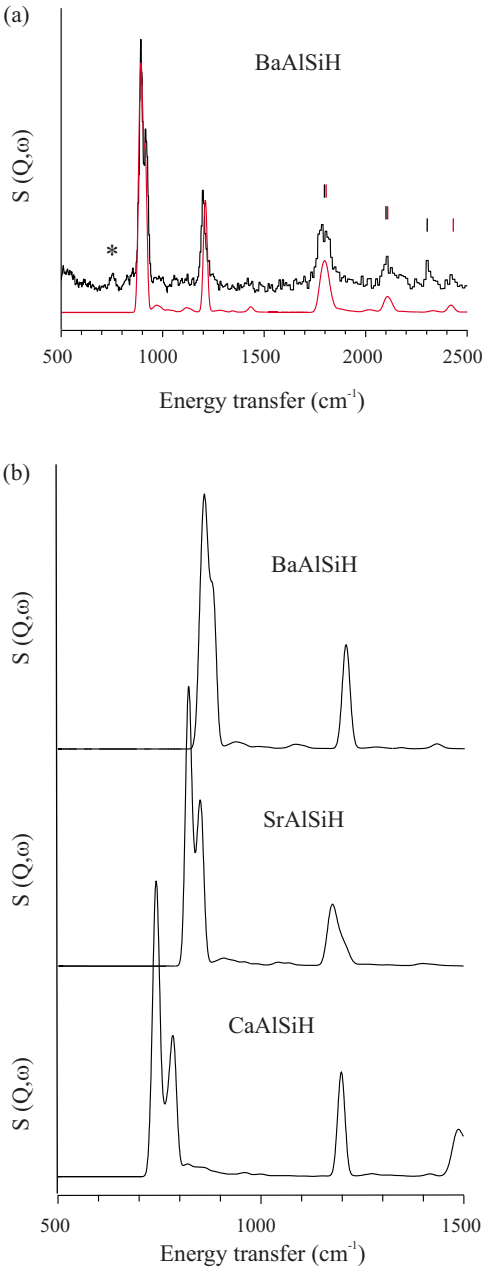

FIG. 8. (Color online) (a) Measured (black line) and calculated [red (gray) line] INS spectra of BaAlSiH. Intensity from the BaH_2 impurity is marked with an asterisk. The calculated frequencies are slightly scaled to achieve agreement of the calculated spectrum with the experimental spectrum. Vertical markers indicate the location of overtone maxima. The calculated spectrum of BaAlSiH based on original frequencies is shown in (b) together with the spectra of SrAlSiH and CaAlSiH.

stretching mode is a direct measure of the Al-H bond strength, whereas the bending mode—where H displaces toward M atoms—reflects indirectly the strength of M-H interactions and will stiffen (i.e., shift to higher frequencies) for stronger M-H interactions. Accordingly, those increase from M=Ca to Ba. However, the Al-H bond is weak as indicated by the low frequency of the stretch compared to other aluminum hydrides,[51] while H is tightly bonded as indicated by the high thermal stability of MAlSiH. Thus, the ionic M-H interactions play an important role in the thermodynamic stability of these hydrides.

IV. CONCLUSIONS

In this work we analyzed the crystal structure, electronic structure, and vibrational property changes connected with the hydrogen-induced metal-nonmetal transition in the systems MAlSi-MAlSiH (M=Ca,Sr,Ba). The peculiarity of this transition is the very small difference between the structures of the AlB_2-type metal and the hydride, which are connected by group-subgroup relations. This, in principle, allows for a second-order-like continuous transition.

The band-gap opening originates in the removal of the partially filled antibonding π^* band in the metals which has predominately Al p_z orbital character. In the hydride this orbital is substantially involved in covalent Al-H bonding and the corresponding states have low energies. The fully occupied bonding π band in the metals turns into flatband below the Fermi level, expressing Si p_z lone-pair states. The dispersion of this band is about 2 eV in CaAlSiH and decreases to about just 1 eV in BaAlSiH. Describing both systems as Zintl phases composed of covalently bonded two-dimensional polyaninons and M^{2+} cations, the metals correspond to electron-excess systems with respect to the optimal electron count of graphitic layers formed by main-group atoms. The hydrides with an additional covalent bond within the polyanionic entity appear electron precise. We propose to describe the Al-H bond in MAlSiH as dative, i.e., [Al $\leftarrow H^{1-}$].

The hydrogenation-induced metal-nonmetal transition has also a decisive consequence on vibrational properties as the soft phonon mode important for the superconducting properties of the metal is removed. This mode is associated with the out-of-plane Al-Si vibration and is most affected by the formation of the Al-H bond. The mode of the Al-Si in-plane vibration, however, is virtually unaffected by hydrogen incorporation, indicating that the Al-Si bond is equally strong in the metallic precursor and the semiconducting hydride. The modes of the Al-H vibrations have frequencies above 700 cm^{-1}. The Al-H stretch is not susceptible to the alkaline-earth counteraction, which indicates a strong integrity of the Al-H bond in the hydrides MAlSiH.

The hydrogenation-induced metal-nonmetal transition described here is characterized by: (1) the small amount of hydrogen involved (25 at. %), (2) the opening of a small band gap, and (3) small unit-cell volume changes ($\Delta V/V$ =2–5 %). This is notably different compared to hitherto reported transitions.[18–22] Potential applications of the reversible transition MAlSi-MAlSiH, however, will be hampered by the relatively high formation and desorption temperatures of the hydrides. On the other hand, the hydrides MAlSiH could reveal interesting properties inherent to the noncentrosymmetric layer structure. Recently it has been suggested that SrAlSiH may be a switchable ferroelectric.[46]

ACKNOWLEDGMENTS

This work was supported by National Science Foundation Grant No. DMR-0638826. Additionally, partial funding by the European Commission DG Research (Contract No. SES6-2006-518271/NESSHY) is acknowledged. We are grateful to Juan Rodriguez-Carvajal for his help with refining the anisotropic peak broadening in the NPD data of CaAlSiH and Stewart Parker at ISIS for his assistance in measuring the INS data of BaAlSiH.

[1] J. Nagamatsu, N. Nakagawa, T. Muranaka, Y. Zenitani, and J. Akimitsu, Nature (London) **410**, 63 (2001).
[2] R. L. Meng, B. Lorenz, Y. S. Wang, J. Cmaidalka, Y. Y. Sun, Y. Y. Xue, J. K. Meen, and C. W. Chu, IEEE Trans. Appl. Supercond. **13**, 3042 (2003).
[3] M. Imai, K. Nishida, T. Kimura, and H. Abe, Appl. Phys. Lett. **80**, 1019 (2002).
[4] M. Imai, K. Nishida, T. Kimura, H. Kitazawa, H. Abe, H. Kito, and K. Yoshii, Physica C **382**, 361 (2002).
[5] B. Lorenz, J. Lenzi, J. Cmaidalka, R. L. Meng, Y. Y. Sun, Y. Y. Xue, and C. W. Chu, Physica C **383**, 191 (2002).
[6] B. Lorenz, J. Cmaidalka, R. L. Meng, and C. W. Chu, Phys. Rev. B **68**, 014512 (2003).
[7] T. Nakagawa, M. Tokunaga, and T. Tamegai, Sci. Technol. Adv. Mater. **7**, S108 (2006).
[8] S. Yamanaka, T. Otsuki, T. Ide, H. Fukuoka, R. Kumashiro, T. Rachi, K. Tanigaki, F. Guo, and K. Kobayashi, Physica C **451**, 19 (2007).
[9] M. Giantomassi, L. Boeri, and G. B. Bachelet, Phys. Rev. B **72**, 224512 (2005).
[10] C. S. Lue, B. X. Xie, and C. P. Fang, Phys. Rev. B **74**, 014505 (2006).
[11] S. Kuroiwa, H. Sagayama, T. Kakiuchi, H. Sawa, Y. Noda, and J. Akimitsu, Phys. Rev. B **74**, 014517 (2006).
[12] K. M. Sparta, R. Müller, M. Merz, G. Roth, P. Adelmann, and T. Wolf, Acta Crystallogr., Sect. B: Struct. Sci. **62**, 710 (2006).
[13] S. Kuroiwa, A. Nakashima, S. Miyahara, N. Furukawa, and J. Akimitsu, J. Phys. Soc. Jpn. **76**, 113705 (2007).
[14] H. J. Choi, D. Roundy, H. Sun, M. L. Cohen, and S. G. Louie, Nature (London) **418**, 758 (2002).
[15] I. I. Mazin and D. A. Papaconstantopoulos, Phys. Rev. B **69**, 180512(R) (2004).
[16] G. Q. Huang, L. F. Chen, M. Liu, and D. Y. Xing, Phys. Rev. B **69**, 064509 (2004).

[17] T. Björling, D. Noréus, K. Jansson, M. Andersson, E. Leonova, M. Edén, U. Hålenius, and U. Häussermann, Angew. Chem., Int. Ed. **44**, 7269 (2005).
[18] J. N. Huiberts, R. Griessen, J. H. Rector, R. J. Wijnaarden, J. P. Dekker, D. G. de Groot, and N. J. Koeman, Nature (London) **380**, 231 (1996).
[19] A. T. M. van Gogh, D. G. Nagengast, E. S. Kooij, N. J. Koeman, J. H. Rector, R. Griessen, C. F. J. Flipse, and R. J. J. G. A. M. Smeets, Phys. Rev. B **63**, 195105 (2001).
[20] A. F. T. Hoekstra, A. S. Roy, T. F. Rosenbaum, R. Griessen, R. J. Wijngaarden, and N. J. Koeman, Phys. Rev. Lett. **86**, 5349 (2001).
[21] T. J. Richardson, J. L. Slack, R. D. Armitage, R. Kostecki, B. Farangis, and M. D. Rubin, Appl. Phys. Lett. **78**, 3047 (2001).
[22] K. Yvon, G. Renaudin, C. M. Wei, and M. Y. Chou, Phys. Rev. Lett. **94**, 066403 (2005).
[23] P.-E. Werner, Ark. Kemi **31**, 513 (1969).
[24] J. Rodriguez-Carvajal, Abstracts of the Satellite Meeting on Powder Diffraction of the XV Congress of the IUCr, Toulouse, France, 1990 (unpublished), p. 127.
[25] G. Kresse and J. Hafner, Phys. Rev. B **47**, 558 (1993); G. Kresse and J. Furthmüller, *ibid.* **54**, 11169 (1996); Comput. Mater. Sci. **6**, 15 (1996).
[26] J. P. Perdew and Y. Wang, Phys. Rev. B **45**, 13244 (1992).
[27] D. Vanderbilt, Phys. Rev. B **41**, 7892 (1990).
[28] P. E. Blöchl, Phys. Rev. B **50**, 17953 (1994); G. Kresse and D. Joubert, *ibid.* **59**, 1758 (1999).
[29] K. Parlinski, Z-.Q. Li, and Y. Kawazoe, Phys. Rev. Lett. **78**, 4063 (1997); K. Parlinski, Z. Q. Li, and Y. Kawazoe, *ibid.* **81**, 3298 (1998).
[30] J.-J. Dong and O. F. Sankey, J. Phys.: Condens. Matter **11**, 6129 (1999); J. Appl. Phys. **87**, 958 (2000); G. S. Nolas, C. A. Kendziora, J. Gryko, J. Dong, C. Myles, A. Poddar, and O. F. Sankey, *ibid.* **92**, 7225 (2002).
[31] R. Heid, K.-P. Bohnen, B. Renker, P. Adelmann, T. Wolf, D. Ernst, and H. Schober, J. Low Temp. Phys. **147**, 375 (2007).
[32] G. Q. Huang, L. F. Chen, M. Liu, and D. Y. Xing, Phys. Rev. B **71**, 172506 (2005).
[33] L. Boeri, J. S. Kim, M. Giantomassi, F. S. Razavi, S. Kuroiwa, J. Akimitsu, and R. K. Kremer, Phys. Rev. B **77**, 144502 (2008).
[34] The ABINIT code is a common project of the Université Catholique de Louvain, Corning Inc., and other contributors; http://www.abinit.org
[35] X. Gonze and C. Lee, Phys. Rev. B **55**, 10355 (1997); X. Gonze, *ibid.* **55**, 10337 (1997).
[36] H. J. Monkhorst and J. D. Pack, Phys. Rev. B **13**, 5188 (1976).
[37] U. Häussermann, F. J. Garcia-Garcia, G. P. Holland, L. L. Daeman, and V. F. Kranak (unpublished).
[38] R.-D. Hoffmann and R. Pöttgen, Z. Kristallogr. **216**, 127 (2001).
[39] T. Sichla and H. Jacobs, Eur. J. Solid State Inorg. Chem. **33**, 453 (1996).
[40] W. Bronger, C. S. Chi, and P. Mueller, Z. Anorg. Allg. Chem. **545**, 69 (1987).
[41] M. Stange, V. Paul-Boncour, M. Latroche, A. Percheron-Guégan, O. Isnard, and V. A. Yartys, J. Alloys Compd. **404-406**, 144 (2005).
[42] H. Wu, W. Zhou, T. J. Udovic, J. J. Rush, and T. Yildirim, Phys. Rev. B **74**, 224101 (2006).
[43] E. A. Leon-Escamilla and J. D. Corbett, Chem. Mater. **18**, 4782 (2006).
[44] I. R. Shein, N. I. Medvedeva, and A. L. Ivansivskii, J. Phys.: Condens. Matter **15**, L541 (2003).
[45] Site-projected densities of states refer to spheres around the atomic sites with radii Ca=1.48 Å, Sr=1.58 Å, Ba=1.75 Å, Al=1.35 Å, Si=1.25 Å, and H=1.1 Å. These correspond to ionic radii for M^{2+} and H^- and covalent radii for Al and Si.
[46] A. Subedi and D. J. Singh, Phys. Rev. B **78**, 045106 (2008).
[47] S. Kuroiwa, A. Q. R. Baron, T. Muranaka, R. Heid, K.-P. Bohnen, and J. Akimitsu, Phys. Rev. B **77**, 140503(R) (2008).
[48] M. H. Lee, O. F. Sankey, T. Björling, D. Moser, D. Noréus, S. F. Parker, and U. Häussermann, Inorg. Chem. **46**, 6987 (2007).
[49] A. J. Ramirez-Cuesta, Comput. Phys. Commun. **157**, 226 (2004); D. Champion, J. Tomkinson, and G. Kearley, Appl. Phys. A: Mater. Sci. Process. **74**, S1302 (2002).
[50] P. C. H. Mitchell, S. F. Parker, A. J. Ramirez-Cuesta, and J. Tomkinson, *Vibration Spectroscopy with Neutrons—With Applications in Chemistry, Biology, Materials Science and Catalysis*, Series on Neutron Techniques and Applications Vol. 3 (World Scientific, Hackensack, NJ, 2005).
[51] Typically molecular or solid-state hydrides with Al-H terminal bonds [e.g., AlH, AlH_2 (C_{2v}), AlH_3 (D_{3h}), AlH_4^- (T_d), and Al_2H_6 (D_{2h}) and $LiAlH_4$ and $NaAlH_4$] display Al-H stretches in the range between 1600 and 1950 cm^{-1}.